Eur. Phys. J. C (2019) 79:399
https://doi.org/10.1140/epjc/s10052-019-6915-0

THE EUROPEAN PHYSICAL JOURNAL C

Regular Article - Theoretical Physics

Susceptibilities and the critical band of crossover region in the QCD phase diagram

Shu-Sheng Xu[1,a], **Pei-Lin Yin**[1,b], **Hong-Shi Zong**[2,3,4,c]

[1] New Energy Technology Engineering Laboratory of Jiangsu Province and School of Science, Nanjing University of Posts and Telecommunications (NJUPT), Nanjing 210023, China
[2] Department of Physics, Nanjing University, Nanjing 210093, China
[3] State Key Laboratory of Theoretical Physics, Institute of Theoretical Physics, CAS, Beijing 100190, China
[4] Joint Center for Particle, Nuclear Physics and Cosmology, Nanjing 210093, China

Received: 1 February 2019 / Accepted: 3 May 2019

Abstract The quark condensate and quark number density are commonly used to determine the QCD phase transition. However, the usually defined quark condensate is divergent in the case of non-chiral limit, and the quark number density suffers from the superficial divergence in numerical calculation. In order to address these issues, we redefine the quark condensate at finite temperature and density and propose a technique to deal with the divergence of the quark condensate and the superficial divergence of the quark number density in numerical calculations. Based on these improvements, we further discuss various susceptibilities as criteria to determine the critical points in the phase transition. It is found that different susceptibilities give different locations of the critical points in the crossover region, which suggests us to define a critical band, instead of some exclusive line in the phase diagram.

1 Introduction

Quantum Chromodynamics (QCD) is the fundamental theory of strong interaction, which describes the interactions between quarks and gluons. Asymptotic freedom [1,2] is the crucial property of QCD, which makes the process of high energy perturbatively calculable. On the other hand, at low temperature and density, the QCD systems have two significant features, i.e., dynamical chiral symmetry breaking (DCSB) and color confinement. As the temperature and (or) density increases, the energy per hadron becomes larger and larger, and the interactions between quarks and gluons become weaker and weaker because of the asymptotic freedom. It is expected that the confinement is relieved and a so-called deconfinement phase transition happens.

Chiral symmetry restoration is another phase transition, which is expected at low and moderate temperature and high density. The quark condensate, $\langle\bar{\psi}\psi\rangle$, is a good indicator for the chiral phase transition and a strict order parameter in the case of chiral limit. The chiral symmetry restoration occurs if the temperature and (or) the density increases so that the condensate, $\langle\bar{\psi}\psi\rangle$, vanishes in the chiral limit. At the same time the effective quark mass also goes to zero. While in the case of finite current quark mass, the usually defined $\langle\bar{\psi}\psi\rangle$ is not a strict order parameter, since it will not go to zero no matter how high the temperature rises. On the other hand, it is believed that there is a crossover region instead of a phase transition at high temperature and low density.

In real QCD, the chiral symmetry is explicitly broken by the finite current quark mass. Thus the quark condensate cannot be regarded as the exact order parameter anymore. But the quark condensate still reflects some important information on QCD phase structure. On the other hand, the temperature susceptibility ($\frac{\partial\langle\bar{\psi}\psi\rangle}{\partial T}$), the chiral susceptibility ($\frac{\partial\langle\bar{\psi}\psi\rangle}{\partial m}$) as well as the quark number susceptibility ($\frac{\partial\langle\psi^{\dagger}\psi\rangle}{\partial\mu}$) are commonly used to determine the critical line in the crossover region of the QCD phase diagram. The peaks of such susceptibilities with respect to the temperature or chemical potential are seen as the critical point. The question whether all these susceptibilities give the same critical line in the QCD phase diagram is often overlooked. In practice, many other susceptibilities, such as topological susceptibility, magnetic susceptibility, spin susceptibility, isospin susceptibility, and charge suscep-

[a] e-mail: xuss@njupt.edu.cn
[b] e-mail: yinpl@njupt.edu.cn
[c] e-mail: zonghs@nju.edu.cn

Published online: 10 May 2019

tibility have been studied in thermal and dense QCD systems [3–9].

There are various theoretical tools and phenomenological models that can be used to study the thermal and dense QCD systems, such as the lattice QCD [10–12], the renormalization group method [13–16], the QCD sum rules [17,18], the NJL model and the Polyakov-loop extended NJL model [19–22]. Compared to other effective models, Dyson-Schwinger equations (DSEs) treat the quarks and gluons as the fundamental degrees of freedom, and feature both the confinement and the DCSB effects. It has provided many insights into the QCD phase diagram [23–29] and hadron properties [30–34]. In this paper, we will use DSEs approach to investigate the chiral phase transition in the strong interaction. As seen below, the commonly defined quark condensate is ultraviolet (UV) divergent, thus a renormalization process is necessary. We will redefine the quark condensate to eliminate UV divergence and be self-consistent with the quark condensate in the case of chiral limit. Various susceptibilities are investigated within the framework of DSEs to determine the critical lines in the crossover region.

The rest of this paper is organized as follows. In Sect. 2, we give a basic introduction to the tools of DSEs at finite temperature and chemical potential and the employed effective interaction model. In Sect. 3, we redefine the quark condensate at finite temperature and chemical potential and propose a new technique to eliminate the (superficial) divergence of the quark condensate and quark number density. We discuss the details of six kinds of susceptibilities in $T-\mu$ plane and compare their peaks in the crossover region. Finally, we give a brief summary in Sect. 4.

2 Dyson–Schwinger equations at finite temperature and density

We first give a brief introduction to DSEs at finite temperature and density. The DSEs are the equations of motion of Green functions in quantum field theory, with the two-point quark propagator being one of the most basic and important Green functions in QCD. In order to study QCD at finite density, one usually introduces a baryon chemical potential μ_B, which is the canonical variable of the baryon number density, based on the law of baryon number conservation. It is convenient to define a quark chemical potential by

$$\mu := \frac{\mu_B}{3}. \tag{1}$$

At finite temperature and density, the DSE for quark propagator is [30]

$$S^{-1}(\vec{p},\tilde{\omega}_n) = S_0^{-1}(\vec{p},\tilde{\omega}_n) + \Sigma(\vec{p},\tilde{\omega}_n), \tag{2}$$

$$S_0^{-1}(\vec{p},\tilde{\omega}_n) = i\vec{\gamma}\cdot\vec{p} + i\tilde{\omega}_n\gamma_4 + m, \tag{3}$$

$$\Sigma(\vec{p},\tilde{\omega}_n) = \sum\!\!\!\!\!\!\int_{\ell,\vec{q}} g^2 D_{\mu\nu}(\vec{p}-\vec{q},\Omega_{n\ell};T,\mu) \times \frac{\lambda^a}{2}\gamma_\mu S(\vec{q},\tilde{\omega}_\ell)\frac{\lambda^a}{2}\Gamma_\nu(\vec{q},\tilde{\omega}_\ell,\vec{p},\tilde{\omega}_n), \tag{4}$$

where

$$\sum\!\!\!\!\!\!\int_{\ell,\vec{q}} := T\sum_{\ell=-\infty}^{\infty}\int\frac{d^3\vec{q}}{(2\pi)^3}. \tag{5}$$

$S_0(\vec{p},\tilde{\omega}_n)$ is the tree-level quark propagator and $\Sigma(\vec{p},\tilde{\omega}_n)$ is the self energy of quark. m is the current quark mass, and we use a typical value $m = 5$ MeV in this work. $D_{\mu\nu}(\vec{p}-\vec{q},\Omega_{n\ell};T,\mu)$ is the dressed gluon propagator and $\Gamma_\nu(\vec{q},\tilde{\omega}_\ell,\vec{p},\tilde{\omega}_n)$ is the dressed quark-gluon vertex. We further have $\tilde{\omega}_n = \omega_n + i\mu$ with $\omega_n = (2n+1)\pi T$ being the Matsubara frequency for fermion and $\Omega_{n\ell} = \omega_n - \omega_\ell$ for boson. In the following, we will use a super-renormalizable interaction model and therefore the renormalization is unnecessary.

The inverse of dressed quark propagator can be expressed as

$$S^{-1}(\vec{p},\tilde{\omega}_n) = i\vec{\not{p}}A(\vec{p},\tilde{\omega}_n) + \mathbf{I}B(\vec{p},\tilde{\omega}_n) + i\tilde{\omega}_n\gamma_4 C(\vec{p},\tilde{\omega}_n) + \vec{\not{p}}\gamma_4\tilde{\omega}_n D(\vec{p},\tilde{\omega}_n). \tag{6}$$

where $\vec{\not{p}} := \vec{\gamma}\cdot\vec{p}$, $\vec{\gamma} = (\gamma_1,\gamma_2,\gamma_3)$, and the four scalar functions $\mathcal{F} = A, B, C, D$ are complex and satisfy

$$\mathcal{F}(\vec{p}^2,\tilde{\omega}_n^2)^* = \mathcal{F}(\vec{p}^2,\tilde{\omega}_{-n-1}^2). \tag{7}$$

The function D is usually negligible since it is power-law suppressed as discussed in Ref. [35]. In particular, D vanishes at $T = \mu = 0$ since it violates the time reversal invariance of quark propgator [36]. The dressed gluon propagator used in this work is

$$g^2 D_{\mu\nu}(\vec{k},\Omega_{n\ell}) = P^T_{\mu\nu}D_T(\vec{k}^2,\Omega_{n\ell}^2) + P^L_{\mu\nu}D_L(\vec{k}^2,\Omega_{n\ell}^2), \tag{8}$$

where $\vec{k} = \vec{p}-\vec{q}$. P^T and P^L are transverse and longitudinal projection operators respectively. Generally speaking, D_T and D_L are not equal at finite temperature and chemical potential, but we take $D_T = D_L$ as an approximation in the region $T < 200$ MeV [37]. We adopt the following ansatz for the scalar function of the gluon propagator

$$D_T = D_L = D_0\frac{\kappa}{\sigma^6}\exp^{-\frac{\kappa}{\sigma^2}}. \tag{9}$$

where $\kappa = \vec{k}^2 + \Omega_{n\ell}^2$. D_0 and σ are model parameters and we use the typical values $D_0 = 0.93$ GeV^2, $\sigma = 0.4$ GeV [38]. For the quark-gluon vertex, we employ the rainbow truncation

$$\Gamma_\nu(\vec{q},\tilde{\omega}_\ell,\vec{p},\tilde{\omega}_n) = \gamma_\nu, \tag{10}$$

which is extensively used in hadron physics and QCD phase diagram study [28,29,38–40].

In the chiral limit, the quark condensate is the exact order parameter for the chiral phase transition. It can be defined as,

$$\langle\bar{\psi}\psi\rangle = -\sum\!\!\!\!\!\!\int_{n,\vec{p}} \mathrm{Tr}[S(\vec{p},\tilde{\omega}_n)]. \tag{11}$$

with the trace over Dirac, color and u-d-flavor indices. Unfortunately, this definition suffers from UV-divergence in the case of finite current quark mass. A commonly used generalization is to renormalize Eq. (11) by subtracting a tree-level quark condensate at finite temperature and chemical potential [41], e.g,

$$\langle\bar{\psi}\psi\rangle_r = -\sum\!\!\!\!\!\!\int_{n,\vec{p}} \mathrm{Tr}[S(\vec{p},\tilde{\omega}_n) - S_0(\vec{p},\tilde{\omega}_n)]. \tag{12}$$

$\langle\bar{\psi}\psi\rangle_r$ goes back to $\langle\bar{\psi}\psi\rangle$ in the chiral limit. However, the drawback of such a definition is that the subtracted term, $S_0(\vec{p},\tilde{\omega}_n)$, brings some additional $T(\mu)$-dependence into the original definition, which will inevitably alter the relevant susceptibilities. In the meantime, there are some other definitions of quark condensate, for instance, authors in Ref. [42] define the quark condensate as

$$\langle\bar{\psi}\psi\rangle^r(T) = \frac{m_f}{m_\pi^4}\left(\langle\bar{\psi}\psi\rangle(T) - \langle\bar{\psi}\psi\rangle(T=0)\right), \tag{13}$$

where m_f and m_π are current quark and pion masses respectively. It is useful to study the susceptibilities related to condensate, but has no direct physical interpretation as the original $\langle\bar{\psi}\psi\rangle$ or $\langle\bar{\psi}\psi\rangle_r$. Based on the above considerations, we propose a definition of quark condensate as

$$\begin{aligned}\langle\bar{\psi}\psi\rangle^R(T,\mu) &= \langle\bar{\psi}\psi\rangle(T,\mu) - \langle\bar{\psi}_0\psi_0\rangle(0,0)\\ &= -\sum\!\!\!\!\!\!\int_{n,\vec{p}} tr[S(\vec{p},\tilde{\omega}_n)] + \int\frac{d^4p}{(2\pi^2)^4} tr[S_0(p)],\end{aligned} \tag{14}$$

where the subscript 0 refers to the quark condensate obtained from a tree-level quark propagator. Here $S_0(p)$ is the tree-level quark propagator at $T=0$ and $\mu=0$. One advantage of this definition is that it coincides with the definition Eq. (11) while m goes to zero, rendering the same meaningful physical interpretation. The other advantage is that Eq. (14) introduces no additional $T(\mu)-$dependence to the quark condensate. So its derivative with respect to T and μ, namely the temperature and vector-scalar susceptibilities which will be defined in the next section, are unchanged by this renormalization procedure. Note that the two terms on the right-hand side of Eq. (14) are individually divergent, but their difference is finite. We develop a calculation technique, which is detailed in Appendix A. In the following, we directly refer to $\langle\bar{\psi}\psi\rangle^R$ as $\langle\bar{\psi}\psi\rangle$ for simiplicity.

Another quantity of interest is the quark number density, which is defined as

$$\begin{aligned}\langle\psi^\dagger\psi\rangle &= -\sum\!\!\!\!\!\!\int_{n,\vec{p}} \mathrm{Tr}[S(\vec{p},\tilde{\omega}_n)\gamma_4]\\ &= -4N_cN_f\sum\!\!\!\!\!\!\int_{n,\vec{p}}\frac{\tilde{\omega}_nC}{\vec{p}^2A^2+\tilde{\omega}_n^2C^2+B^2}.\end{aligned} \tag{15}$$

The quark number density is well defined even in the case of finite current quark mass, but this formula confronts a numerical computation difficulty. We can see from Eq. (15) that the UV-behavior of integrand is $\frac{1}{\vec{p}^2}$ and $\frac{1}{\tilde{\omega}_n}$, hence the summation and integration are superficially divergent. By the way, the lattice QCD has also investigated this problem in studying the quark number susceptibility recently [43]. The non-interacting fermion quark number susceptibility is subtracted so that the numerical calculation converges. In this connection, we develop a novel technique, which is detailed in Appendix A, to handle the numerical computation without trouble.

3 Susceptibilities and crossover region

In the chiral limit, the quark condensate is the exact order parameter for the chiral phase transition. It still plays an important role beyond the chiral limit, since it is the first order derivative of the pressure with respect to the current quark mass m

$$\langle\bar{\psi}\psi\rangle = -\frac{T}{V}\frac{\partial\ln\mathcal{Z}}{\partial m}. \tag{16}$$

Its discontinuity is a criterion of the first order phase transition. The quark number density, on the other hand, is proportional to the derivative of pressure with respect to the chemical potential

$$\langle\psi^\dagger\psi\rangle = \frac{T}{V}\frac{\partial\ln\mathcal{Z}}{\partial\mu}, \tag{17}$$

which is another important quantity in thermal and dense QCD systems. For the sake of comparison, we display $\langle\bar{\psi}\psi\rangle$ and $\langle\psi^\dagger\psi\rangle$ varying with μ at different T in Fig. 1. At $T=120$ MeV, both $\langle\bar{\psi}\psi\rangle$ and $\langle\psi^\dagger\psi\rangle$ show discontinuities at a critical chemical potential, namely, $\mu_c = 160$ MeV. It implies that a first order phase transition happens, and these two different criteria give the same phase transition point, which is consistent with the model independent study in Ref. [44]. It is interesting that the quark number density is almost zero below μ_c at low temperature. As temperature increases, the discontinuities of both $\langle\bar{\psi}\psi\rangle$ and $\langle\psi^\dagger\psi\rangle$ disappear at $T = 129$ MeV, and a very rapidly changing area occurs. As the temperature increases further, the $\langle\bar{\psi}\psi\rangle$ and $\langle\psi^\dagger\psi\rangle$

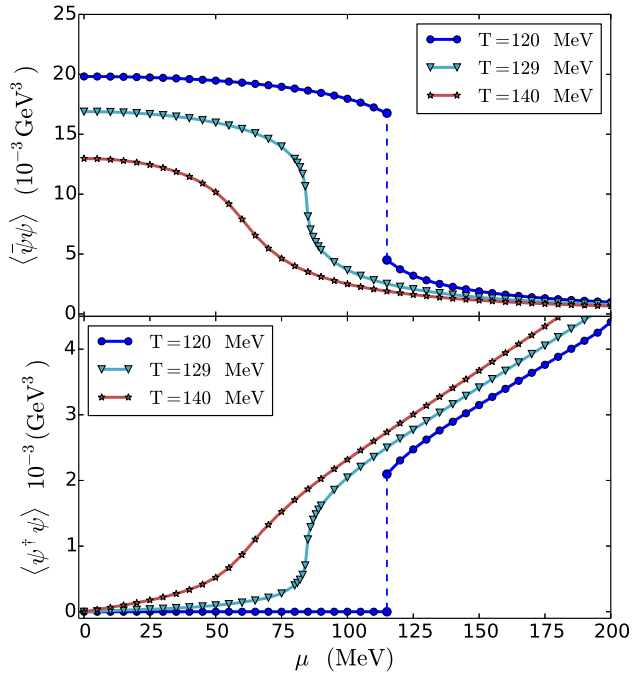

Fig. 1 The quark condensate and quark number density varying with μ at $T = 110$ MeV, $T = 120$ MeV, $T = 129$ MeV and $T = 140$ MeV, respectively

vary smoothly with μ. In order to have a deeper insight into these transition behaviors, we resort to susceptibilities in the following.

Let's introduce six kinds of susceptibilities in thermal and dense QCD systems: the chiral susceptibility χ_s, the quark number susceptibility χ_q, the thermal susceptibility χ_T, the frequently used vector-scalar susceptibility χ_μ, and two additional χ_{vT}, χ_m for completeness. They are defined as

$$\chi_s = -\frac{\partial\langle\bar{\psi}\psi\rangle}{\partial m}, \tag{18}$$

$$\chi_\mu = \frac{\partial\langle\bar{\psi}\psi\rangle}{\partial\mu}, \tag{19}$$

$$\chi_T = \frac{\partial\langle\bar{\psi}\psi\rangle}{\partial T}, \tag{20}$$

$$\chi_m = -\frac{\partial\langle\psi^\dagger\psi\rangle}{\partial m}, \tag{21}$$

$$\chi_q = \frac{\partial\langle\psi^\dagger\psi\rangle}{\partial\mu}, \tag{22}$$

$$\chi_{vT} = \frac{\partial\langle\psi^\dagger\psi\rangle}{\partial T}. \tag{23}$$

Actually the χ_μ and χ_m are identical since

$$\chi_\mu = \frac{\partial\langle\bar{\psi}\psi\rangle}{\partial\mu} = -\frac{T}{V}\frac{\partial^2\ln\mathcal{Z}}{\partial m\partial\mu} = -\frac{\partial\langle\psi^\dagger\psi\rangle}{\partial m} = \chi_m. \tag{24}$$

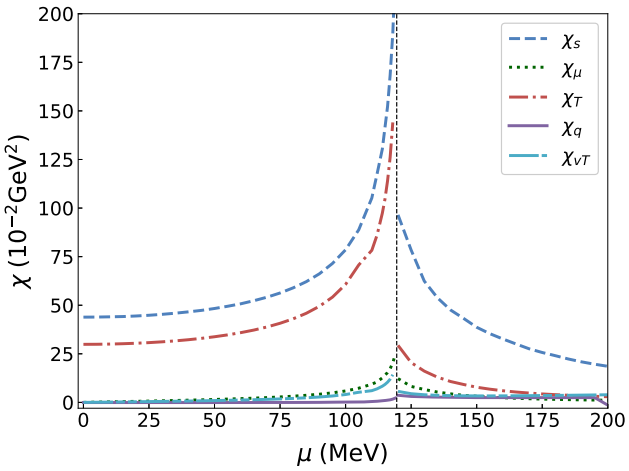

Fig. 2 Five different susceptibilities at $T = 120$ MeV

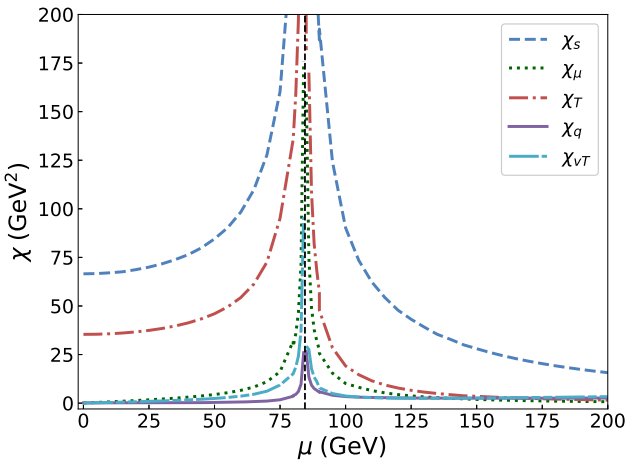

Fig. 3 Five different susceptibilities at $T = 129$ MeV

We first display the five susceptibilities at $T = 120$ MeV in Fig. 2. Apparently, all the susceptibilities share the same discontinuity point at $\mu = 119$ MeV. Their behaviors around the critical point are very similar. One can see that the values at both sides for them are finite and unequal to each other, which reflects the discontinuity of the quark condensate and quark number density. It is the typical feature of the first order phase transition.

In Fig. 1, both $\langle\bar{\psi}\psi\rangle$ and $\langle\psi^\dagger\psi\rangle$ have a continuous but rapidly changing area at $T = 129$. Whether this is the second order phase transition point can be confirmed with the help of susceptibilities. Figure 3 shows the susceptibilities varying with μ at $T = 129$ MeV, all of which tend to infinity for both sides at $\mu = 85$ MeV. Since Fig. 1 has already shown that the $\langle\bar{\psi}\psi\rangle$ and $\langle\psi^\dagger\psi\rangle$ are both continuous at $\mu = 85$ MeV and $T = 129$ MeV, this is actually the second order phase transition point. We now conclude that various susceptibilities give the same location of the first order and the second order phase transition points in thermal and dense QCD system.

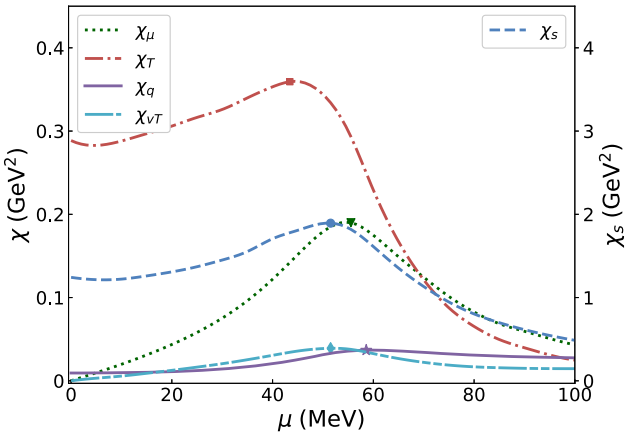

Fig. 4 Five different susceptibilities at $T = 145$ MeV. χ_s is plotted with right vertical axis, and $\chi_\mu, \chi_T, \chi_q, \chi_{vT}$ are plotted with left vertical axis

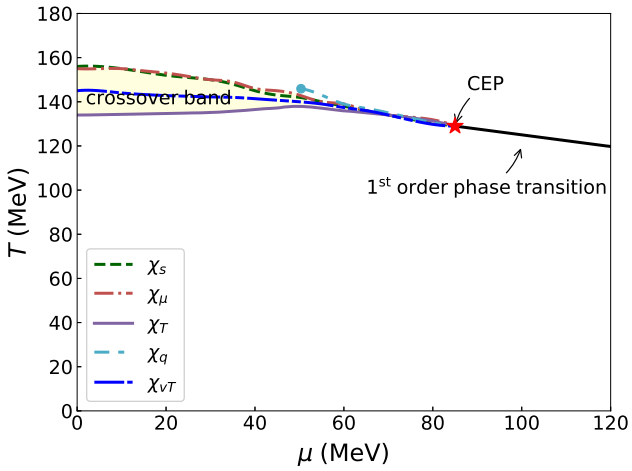

Fig. 5 The critical band of the QCD phase diagram

While $T > 129$ MeV, the system enters the continuous transition region, namely, the crossover region. The five susceptibilities varying with μ at $T = 145$ MeV are displayed in Fig. 4. At low chemical potential region, two of the susceptibilities, namely, χ_μ and χ_{vT}, vanish at $\mu = 0$ since the quark number density vanishes at $\mu = 0$ at any temperature and current quark mass, which can be partially seen from Fig. 1. In terms of the critical behavior, they behave very similarly, they all contain a peak at some critical chemical potential. However, the peaks of different susceptibilities are located at different points, which have been marked in Fig. 4. We can see from Fig. 4 that for $T = 145$ MeV the peaks of χ_s, χ_μ, χ_T, χ_q, χ_{vT} are located at $\mu_c = 51$ MeV, $\mu_c = 55$ MeV, $\mu_c = 43$ MeV, $\mu_c = 58$ MeV, $\mu_c = 51$ MeV, respectively. We extract all such critical points for all the temperatures in the crossover region and plot the phase diagram in Fig. 5. We can see from Fig. 5 that the critical lines of χ_s and χ_μ are very close, and their critical temperatures for certain μ are larger than those of χ_T and χ_{vT}. The χ_T poses the lowest critical temperature for certain μ and the critical line of χ_{vT} is located between them. It is worth noting that the critical line of χ_q ends at $(T, \mu) = (45, 146)$ MeV because the χ_q is monotonically increasing with μ and T in the region of high temperature and low chemical potential. We display a band spanned by these critical lines, which implies that the critical band is more suitable for the crossover region.

4 Summary

We have studied the chiral phase transition with the help of quark condensate and quark number density in the framework of Dyson–Schwinger equations. A renormalized definition of the quark condensate in the case of beyond chiral limit is proposed in a self-consistent way. And we suggest a numerical technique to deal with the superficial divergence in the calculation of the quark number density.

The first order phase transition is located at the same points by these two different quantities, i.e, quark condensate and quark number density, which is consistent with the model independent study. Various susceptibilities are used to determine the critical line in the crossover region. Five susceptibilities give different critical lines. The critical line of quark number susceptibility ends at $(T, \mu) = (45, 146)$ MeV because it monotonically increases with μ in the region of $\mu < 45$ MeV. The critical lines of χ_s and χ_μ are very close and their T_c are larger than those of other susceptibilities at a certain μ. The χ_T has the lowest T_c. Therefore we suggest a critical band in the crossover region, where χ_s and χ_T give the upper and lower boundaries respectively.

Acknowledgements We acknowledge the fruitful discussions with Yilun Du. This work is supported in part by the National Natural Science Foundation of China (under Grants no. 11847024, no. 11747140, no. 11475085, no. 11535005, no. 11690030, no. 11873030), Nanjing University of Posts and Telecommunications Science Foundation (Grant no. NY219032, and no. NY218132), the Fundamental Research Funds for the Central Universities (under Grant no. 020414380074), the Natural Science Foundation of Jiangsu Province of China (under Grant no. BK20180738), and by the National Major state Basic Research and Development of China (Grant no. 2016YFE0129300).

Data Availability Statement This manuscript has no associated data or the data will not be deposited. [Authors' comment: The data of the main results are described in the manuscript, and also displayed in figures.]

Appendix A: Techniques to calculate condensate and quark number density

The quark condensate in the case of non-zero quark mass is divergent. Hence some subtraction is necessary. In our study, we define the quark condensate as

$$\langle\bar{\psi}\psi\rangle^R(T,\mu) := \langle\bar{\psi}\psi\rangle(T,\mu) - \langle\bar{\psi}_0\psi_0\rangle(0,0). \tag{A1}$$

If one calculates the two terms in Eq. (A1) respectively, they are both divergent. Actually, We can make use of the condensate of free quark at finite temperature and finite chemical potential $\langle\bar{\psi}_0\psi_0\rangle(T,\mu)$ twice to eliminate their divergence. Specifically,

$$\begin{aligned}
&\langle\bar{\psi}\psi\rangle^R(T,\mu)\\
&= \langle\bar{\psi}\psi\rangle(T,\mu) - \langle\bar{\psi}_0\psi_0\rangle(T,\mu) + \langle\bar{\psi}_0\psi_0\rangle(T,\mu)\\
&\quad - \langle\bar{\psi}_0\psi_0\rangle(0,0)\\
&= -N_f N_c \sum\!\!\!\!\!\!\int_{n,\vec{p}} \left(\frac{4B}{\vec{p}^2A^2 + \tilde{\omega}_n^2 C^2 + B^2} - \frac{4m}{\vec{p}^2 + \tilde{\omega}_n^2 + m^2} \right)\\
&\quad - N_f N_c \int \frac{d^3p}{(2\pi)^3} \left(T \sum_{n=-\infty}^{\infty} \frac{4m}{\vec{p}^2 + \tilde{\omega}_n^2 + m^2} \right.\\
&\quad \left. - \int \frac{dp_4}{2\pi} \frac{4m}{\vec{p}^2 + p_4^2 + m^2} \right)\\
&= -N_f N_c \sum\!\!\!\!\!\!\int_{n,\vec{p}} \left(\frac{4B}{\vec{p}^2A^2 + \tilde{\omega}_n^2 C^2 + B^2} \right.\\
&\quad \left. - \frac{4m}{\vec{p}^2 + \tilde{\omega}_n^2 + m^2} \right)\\
&\quad - N_f N_c \int \frac{d^3p}{(2\pi)^3} \left(\tanh(\frac{\sqrt{\vec{p}^2 + m^2}}{2T}) - 1 \right).
\end{aligned} \tag{A2}$$

In this way, both numerical integrations can converge very quickly.

The technique to calculate quark number density is similar. By denoting $\langle\psi^\dagger\psi\rangle(T,\mu,m)$ as the quark number density with T,μ and m, we have

$$\begin{aligned}
&\langle\psi^\dagger\psi\rangle(T,\mu,m)\\
&= \langle\psi^\dagger\psi\rangle(T,\mu,m) - \langle\psi^\dagger\psi\rangle(T,\mu,0) + \langle\psi^\dagger\psi\rangle(T,\mu,0)\\
&= \langle\psi^\dagger\psi\rangle(T,\mu,m) - \langle\psi_0^\dagger\psi_0\rangle(T,\mu,0) + \langle\psi_0^\dagger\psi_0\rangle(T,\mu,m)\\
&\quad - \langle\psi^\dagger\psi\rangle(0,0,0) + \langle\psi^\dagger\psi\rangle(T,\mu,0)\\
&= -N_f N_c \sum\!\!\!\!\!\!\int_{n,\vec{p}} \left(\frac{4\tilde{\omega}_n C}{\vec{p}^2A^2 + \tilde{\omega}_n^2 C^2 + B^2} - \frac{4\tilde{\omega}_n}{\vec{p}^2 + \tilde{\omega}_n^2 + m^2} \right)\\
&\quad - N_f N_c \sum\!\!\!\!\!\!\int_{n,\vec{p}} \left(\frac{4\tilde{\omega}_n}{\vec{p}^2 + \tilde{\omega}_n^2 + m^2} - \frac{4\tilde{\omega}_n}{\vec{p}^2 + \tilde{\omega}_n^2} \right)\\
&\quad + N_f N_c \left(\frac{T^2\mu}{3} + \frac{\mu^3}{3\pi^2} \right)
\end{aligned}$$

$$\begin{aligned}
&= -N_f N_c \sum\!\!\!\!\!\!\int_{n,\vec{p}} \left(\frac{4\tilde{\omega}_n C}{\vec{p}^2A^2 + \tilde{\omega}_n^2 C^2 + B^2} \right.\\
&\quad \left. - \frac{4\tilde{\omega}_n}{\vec{p}^2 + \tilde{\omega}_n^2 + m^2} \right)\\
&\quad - N_f N_c \int \frac{d^3p}{(2\pi)^3} \left[\tanh\left(\frac{\sqrt{\vec{q}^2 + m^2} - \mu}{2T} \right) \right.\\
&\quad - \tanh\left(\frac{\sqrt{\vec{q}^2} - \mu}{2T} \right)\\
&\quad \left. - \tanh\left(\frac{\sqrt{\vec{q}^2 + m^2} + \mu}{2T} \right) + \tanh\left(\frac{\sqrt{\vec{q}^2} + \mu}{2T} \right) \right]\\
&\quad + N_f N_c \left(\frac{T^2\mu}{3} + \frac{\mu^3}{3\pi^2} \right).
\end{aligned} \tag{A3}$$

These two numerical integrations can converge very quickly too.

References

1. D.J. Gross, F. Wilczek, Phys. Rev. Lett. **30**, 1343 (1973)
2. H.D. Politzer, Phys. Rev. Lett. **30**, 1346 (1973)
3. B. Alls, M. D'Elia, A.D. Giacomo, Phys. Lett. B **483**, 139 (2000)
4. H.-C. Kim, M. Musakhanov, M. Siddikov, Phys. Lett. B **608**, 95 (2005)
5. F. Karsch, E. Laermann, Phys. Rev. D **50**, 6954 (1994)
6. R.V. Gavai, S. Gupta, P. Majumdar, Phys. Rev. D **65**, 054506 (2002)
7. Y.-L. Du, Z.-F. Cui, Y.-H. Xia, H.-S. Zong, Phys. Rev. D **88**, 114019 (2013)
8. Y.-L. Du, Y. Lu, S.-S. Xu, Z.-F. Cui, C. Shi, H.-S. Zong, Int. J. Mod. Phys. **A30**, 1550199 (2015). arXiv:1506.04368 [hep-ph]
9. P.-L. Yin, Y.-M. Shi, Z.-F. Cui, H.-T. Feng, H.-S. Zong, Phys. Rev. D **90**, 036007 (2014)
10. Z. Fodor, S.D. Katz, JHEP **2004**, 050 (2004)
11. S. Borsanyi, Z. Fodor, C. Hoelbling, S.D. Katz, S. Krieg, C. Ratti, K.K. Szabo (Wuppertal-Budapest), JHEP **09**, 073 (2010). arXiv:1005.3508 [hep-lat]
12. S. Ejiri, N. Yamada, Phys. Rev. Lett. **110**, 172001 (2013)
13. F. Wilczek, Int. J. Mod. Phys. A **7**, 3911 (1992)
14. A. Ali Khan, S. Aoki, R. Burkhalter, S. Ejiri, M. Fukugita, S. Hashimoto, N. Ishizuka, Y. Iwasaki, K. Kanaya, T. Kaneko, Y. Kuramashi, T. Manke, K. Nagai, M. Okamoto, M. Okawa, A. Ukawa, T. Yoshié (CP-PACS Collaboration), Phys. Rev. D **63**, 034502 (2000)
15. B.J. Schaefer, J. Wambach, Phys. Particles Nuclei **39**, 1025 (2008)
16. J.O. Andersen, W.R. Naylor, A. Tranberg, JHEP **2014**, 187 (2014)
17. A. Ayala, C. Dominguez, M. Loewe, Adv. High Energy Phys. **2017**, 9291623
18. A. Ayala, C.A. Dominguez, L.A. Hernandez, M. Loewe, J.C. Rojas, C. Villavicencio, Phys. Rev. D **92**, 016006 (2015)
19. S.P. Klevansky, Rev. Mod. Phys. **64**, 649 (1992)
20. M. Buballa, Phys. Rep. **407**, 205 (2005)
21. Z.-F. Cui, J.-L. Zhang, H.-S. Zong, Sci. Rep. **7**, 45937 (2017)
22. Z. Pan, Z.-F. Cui, C.-H. Chang, H.-S. Zong, Int. J. Mod. Phys. **A32**, 1750067 (2017). arXiv:1611.07370 [hep-ph]
23. C.S. Fischer, J. Luecker, C.A. Welzbacher, Phys. Rev. D **90**, 034022 (2014)
24. C.S. Fischer, J. Luecker, J.M. Pawlowski, Phys. Rev. D **91**, 014024 (2015)

25. C.S. Fischer, J. Luecker, C.A. Welzbacher, Nuclear Physics A **931**, 774 (2014), qUARK MATTER 2014
26. S.-S. Xu, Z.-F. Cui, B. Wang, Y.-M. Shi, Y.-C. Yang, H.-S. Zong, Phys. Rev. D **91**, 056003 (2015)
27. S.-S. Xu, Y.-M. Shi, Y.-C. Yang, Z.-F. Cui, H.-S. Zong, Chin. Phys. Lett. **32**, 121203 (2015)
28. F. Gao, Y.-X. Liu, Phys. Rev. D **94**, 094030 (2016)
29. F. Gao, Y.-X. Liu, Phys. Rev. D **94**, 076009 (2016)
30. C.D. Roberts, A.G. Williams, Prog. Part. Nucl. Phys. **33**, 477 (1994)
31. P. Maris, C.D. Roberts, P.C. Tandy, Phys. Lett. B **420**, 267 (1998)
32. P. Maris, C.D. Roberts, Int. J. Mod. Phys. E **12**, 297 (2003)
33. G. Eichmann, I.C. Cloët, R. Alkofer, A. Krassnigg, C.D. Roberts, Phys. Rev. C **79**, 012202 (2009)
34. G. Eichmann, R. Alkofer, A. Krassnigg, D. Nicmorus, Phys. Rev. Lett. **104**, 201601 (2010)
35. C. Roberts, S. Schmidt, Prog. Part. Nucl. Phys. **45**, S1 (2000)
36. J.J. Rusnak, R.J. Furnstahl, Zeitschrift für Physik A Hadrons and Nuclei **352**, 345 (1995)
37. A. Cucchieri, A. Maas, T. Mendes, Phys. Rev. D **75**, 076003 (2007)
38. P. Maris, P.C. Tandy, Phys. Rev. C **60**, 055214 (1999)
39. P. Maris, C.D. Roberts, P.C. Tandy, Phys. Lett. B **420**, 267 (1998). arXiv:nucl-th/9707003 [nucl-th]
40. P. Maris, C.D. Roberts, Phys. Rev. C **56**, 3369 (1997)
41. C. Shi, Y.-L. Wang, Y. Jiang, Z.-F. Cui, H.-S. Zong, JHEP **2014**, 14 (2014)
42. G. Bali, F. Bruckmann, G. Endrődi, Z. Fodor, S. Katz, S. Krieg, A. Schäfer, K. Szabo, JHEP **2012**, 44 (2012)
43. R.V. Gavai, S. Sharma, Phys. Lett. B **749**, 8 (2015)
44. A. Barducci, R. Casalbuoni, G. Pettini, R. Gatto, Phys. Lett. B **301**, 95 (1993). arXiv:hep-ph/9212276 [hep-ph]